Measurement of highly non-uniform residual stress fields with reduced plastic error

H.K. Kim, H.E. Coules, M.J. Pavier, A. Shterenlikht

Abstract

Experimental validations of a recently proposed method for residual stress measurement are presented. The method, specifically designed for highly non-uniform in-plane residual stress fields is applied in this work to measure the residual stresses resulting from four-point bend of an Aluminium 7075-T6 bar. The benefit of the method is that it can reconstruct stress fields without any assumptions of in-plane uniformity. The method uses two cuts, propagated from both side surfaces and collection of full-field relaxation displacement fields from side surfaces using 2D high-resolution digital image correlation (DIC). The reconstructed residual stress agrees well with that predicted by FE modelling and neutron diffraction measurement. In addition, it is shown that induced plastic strain during the relaxation process, which reduces accuracy of the method, is strongly influenced by the direction of the propagation of the cut. This implies that it is possible to reduce substantially plastic strain during cutting if the orientation and propagation of the cut is carefully chosen.

1 Introduction

Mechanical strain relaxation (MSR) is a name given to a group of destructive techniques for the measurement of residual stress. Many such techniques have been developed, and applied to a great variety of engineering components. All MSR techniques involve removing some stressed material and then measuring the deformations produced by the removal of that material. Such deformation (strain or displacement) are typically measured with strain gauges. More recently non-contact optical techniques have been applied due to their ability to record

full-field data. Popular optical methods include holographic and electronic speckle pattern interferometry (ESPI) [1] , Moiré interferometry [2] and Digital Image Correlation (DIC) [3]. The measured strain or displacement fields are converted to stress using inverse elastic models [4].

Although these general principles of measuring residual stress have been applied to a wide range of specimen geometries and engineering materials, their successful implementation depends on two key assumptions: (1) relaxation is purely elastic i.e. no plastic flow on relaxation, and (2) a uniform stress field, at least on some plane or in some direction. In many practical applications these assumptions are known not to be true. In particular, significant plastic flow accompanies relaxation when the magnitude of the residual stress is close to yield. These may be the most important cases for experimental residual stress analysis [5–7].

Residual stress levels as low as 0.4 of the yield stress have been shown to present significant challenges to hole drilling methods, due to plastic deformation caused by stress redistribution upon hole drilling [7]. Although there have been some efforts to introduce plastic error corrections, to mitigate the errors introduced into the reconstructed stresses due to plastic flow, the issue is far from being resolved [7–9].

Assumptions about the shape of the residual stress fields are invariably made. Of these the most frequent is the assumption of stress uniformity in some plane, that allows the use of established closed form analytical elastic solutions. For example, the analytical model used in the hole drilling technique is a hole in a 2D plate under uniform far field stress. In the case of the deep hole drilling method [7], the stress field is assumed uniform in the plane normal to the axis of the cut. The contour method is a notable exception: there is no assumption about the shape of the residual stress field [10].

In this work, we first provide numerical (Sec. 3) and experimental (Sec. 4) validation of a recently proposed method suitable for arbitrary non-uniform stress fields [11] (Sec. 2) with a well controlled four point bend residual stress field (Sec. 3.2). Then, we focus on the idea of reducing the plasticity effect by carefully choosing the direction and propagation of the cut (Sec. 6). The method is shown to reconstruct the predicted residual stress well. In addition it is shown that this method can be made to induce very little plastic strain.

2 The analytical model

The elastic analytical model used in this work is the problem of a 2D semi-infinite strip of width $2c$, with self-equilibrated traction loading at one end, see Fig. 1(a). This analytical model will be employed for measuring residual stress profile in a four point bend bar, see Fig. 1(b). The zigzag residual stress profile is generated by a four-point bend elastic-plastic loading sequence [12], followed by sectioning the specimen in the midsection of the longitudinal direction of the bar. Then, the analytical model can be used to reconstruct residual stress profile along the symmetry line, $x_1 = 0$, from the relaxation displacements measured on the free surface. The use of a free surface for data collection implies the assumption of the plane stress condition in the analytical model. However, the residual stress at the surface differs from that in the interior. This can lead to errors in the reconstructed residual stress. Indeed, this problem does occur as will be discussed later in Sec. 5 and 7.

The solution to the elastic problem is due to Mathieu [13, p.61]. The application of Math-

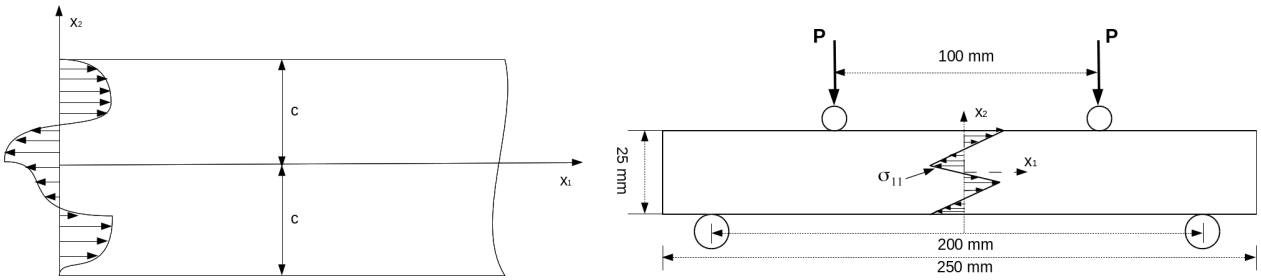

Figure 1: (a) Schematic of the problem geometry for a 2D semi-infinite rectangular strip of width $2c$. Arbitrary self-equilibrated loading is applied at one end ($x_1 = 0$). (b) Schematic diagram of a four-point bend test used in this work. The beam is deformed plastically and then unloaded. This creates a reproducible residual stress field between the inner rollers. The specimen is then cut with wire EDM on the $x_1 = 0$ symmetry plane. This releases the residual stresses.

ieu's solution to residual stress measurement was first investigated in [11], where the authors show how various types of relaxation data could be used: in-plane displacements, out-of-plane displacements, photo-elastic data and strain. Here we give a brief description of the method, specifically with in-plane relaxation displacements in mind.

The following even and odd stress functions can be easily shown to satisfy the bi-harmonic

equation:

$$f = e^{-\gamma x_1/c}\left(\xi \cos\frac{\gamma x_2}{c} + \frac{\gamma x_2}{c}\sin\frac{\gamma x_2}{c}\right); \qquad g = e^{-\phi x_1/c}\left(\psi \sin\frac{\phi x_2}{c} + \frac{\phi x_2}{c}\cos\frac{\phi x_2}{c}\right) \tag{1}$$

where $2c$ is the strip width, see Fig. 1(a), x_1 is along the strip and x_2 is normal to the strip axis. The boundary conditions are: $\sigma_{22} = \sigma_{12} = 0$ at $x_2 = \pm c$; $\int_{-c}^{c} \sigma_{11} \mathrm{d}x_2 = \int_{-c}^{c} \sigma_{12} \mathrm{d}x_2 = 0$ at $x_1 = 0$. The boundary conditions are satisfied if $f = \frac{\partial f}{\partial x_2} = 0$ at $x_2 = \pm c$, which leads to the following equations for the unknown dimensionless parameters of the stress functions, γ, ξ, ϕ, ψ:

$$\sin 2\gamma + 2\gamma = 0; \qquad \xi = -\gamma \tan\gamma; \qquad \sin 2\phi - 2\phi = 0; \qquad \psi = -\phi/\tan\phi \tag{2}$$

which have an infinite number of solutions. The first non-zero roots are: $\gamma_1 = 2.106$, $\xi_1 = 1.125$, $\phi_1 = 3.749$, $\psi_1 = 1.384$. Combining the even and the odd stress functions using the infinite number of γ and ϕ roots, we construct the infinite series representation of the stress function, suitable for any arbitrary self-equilibrated loading at the $x_1 = 0$ boundary:

$$\theta = \sum_{i=1}^{\infty} a_i \Re(f_i) + b_i \Im(f_i) + c_i \Re(g_i) + d_i \Im(g_i) \tag{3}$$

As both f and g stress functions satisfy the bi-harmonic equation, the direct and shear components of stress are determined from θ:

$$\sigma_{11} = \frac{\partial^2 \theta}{\partial x_2^2} \qquad \sigma_{22} = \frac{\partial^2 \theta}{\partial x_1^2} \qquad \tau_{12} = \frac{\partial^2 \theta}{\partial x_1 \partial x_2} \tag{4}$$

By applying Hooke's law for plane stress and small strain theory to (4), one can represent the measured in-plane displacements at any point on the surface via functions of the unknown coefficients, $a_i, b_i, c_i, d_i, i = 1, 2, \ldots, \infty$, and several position dependent integrals:

$$
\begin{aligned}
Eu_1 = \quad & \sum_{i=1}^{\infty} a_i \int \Re\left(\frac{\partial^2 f_i}{\partial x_2^2} - \nu\frac{\partial^2 f_i}{\partial x_1^2}\right) dx_1 + b_i \int \Im\left(\frac{\partial^2 f_i}{\partial x_2^2} - \nu\frac{\partial^2 f_i}{\partial x_1^2}\right) dx_1 \\
& + c_i \int \Re\left(\frac{\partial^2 g_i}{\partial x_2^2} - \nu\frac{\partial^2 g_i}{\partial x_1^2}\right) dx_1 + d_i \int \Im\left(\frac{\partial^2 g_i}{\partial x_2^2} - \nu\frac{\partial^2 g_i}{\partial x_1^2}\right) dx_1 \\
Eu_2 = \quad & \sum_{i=1}^{\infty} a_i \int \Re\left(\frac{\partial^2 f_i}{\partial x_1^2} - \nu\frac{\partial^2 f_i}{\partial x_2^2}\right) dx_2 + b_i \int \Im\left(\frac{\partial^2 f_i}{\partial x_1^2} - \nu\frac{\partial^2 f_i}{\partial x_2^2}\right) dx_2 \\
& + c_i \int \Re\left(\frac{\partial^2 g_i}{\partial x_1^2} - \nu\frac{\partial^2 g_i}{\partial x_2^2}\right) dx_2 + d_i \int \Im\left(\frac{\partial^2 g_i}{\partial x_1^2} - \nu\frac{\partial^2 g_i}{\partial x_2^2}\right) dx_2
\end{aligned}
\tag{5}
$$

Now the problem is the standard Linear least square (LLS) problem:

$$
\min_x ||\mathbf{Ax} - \mathbf{u}||_2 \tag{6}
$$

where $\mathbf{x} = (a_1, b_1, c_1, d_1, \ldots a_N, b_N, c_N, d_N)^T$ is the vector of unknown coefficients for the terms in the Mathieu series, $4N$ long. $\mathbf{u}$ is the vector of measured in-plane relaxation displacements, $2M$ long, M is the number of measured displacement points (two displacements, u_1 and u_2 are measured at each point) and $\mathbf{A}$ is a matrix of integral functions of f and g taken at the locations of the measurement points. As always for the stability of LLS, $M \gg N$. Finally, the stresses at $x_1 = 0$ are calculated from the stress function, θ.

3 FE experiments

3.1 Validation of the analytical model

Before deploying the analytical model in an experiment, it was validated numerically using FE simulation. Different self-equilibrating stress fields were applied at one end of the 2D rectangular strip of the FE model. The calculated displacement fields were used as the input for Eqn. (6). After the series coefficients were calculated, the boundary stress profile was reconstructed and compared against that applied originally to the FE model. The model is considered validated if the error between the applied and reconstructed boundary stresses is small for a variety of stress profiles.

Fig. 2 shows that the validation was successful. Fig. 2a shows the case of a sinusoidal stress

profile. There is an excellent agreement between the applied and the reconstructed σ_{11}, σ_{22} and σ_{12} profiles. The maximum absolute error was 11.77 MPa and the root-mean-square(RMS) error in the σ_{11} distribution of the peak value was approximately 0.86%. Fig. 2b shows a stress profile with discontinuities. These discontinuities were turned into finite gradients (although high) by finite element discretisation. The agreement is not as good as for the smooth sinusoid fields, particularly at the points of discontinuity. However, this is a known phenomenon, usually attributed to Gibbs in representing discontinuities by Fourier series [14]. The general agreement is very good.

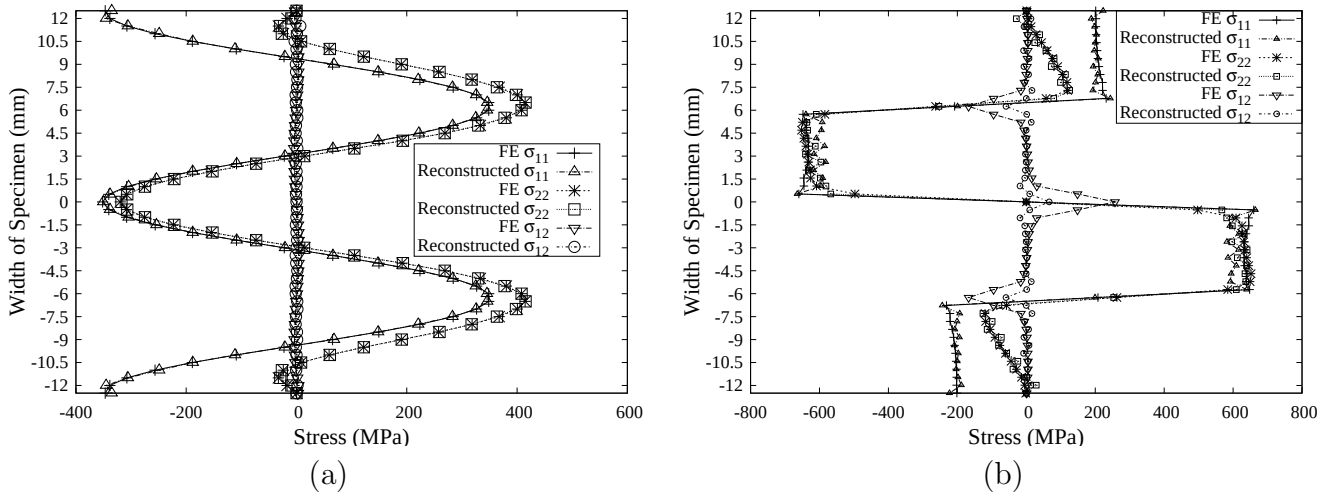

Figure 2: FE validation of reconstructed residual stress fields, showing: (a) a sinusoidal loading, and (b) loading with discontinuities.

3.2 Four-point bend simulation

2D finite element simulation of the four-point bend test was carried out to simulate the experimental measurement. A 2D model of half length of the specimen, 125×25 mm^2, was generated with the longitudinal symmetry condition on the left end ($x_1 = 0$). No clamping was used in the experiment, hence the symmetry condition in the model is correct. A single node, at the corner furthest from the symmetry line, was constrained to prevent the rigid body motion in the model. The EDM cutting process was simulated by removing the longitudinal symmetry condition on the nodes instantaneously. The Abaqus finite element code [15] was employed using 9678 eight-node quadratic plane stress quadrilateral elements with reduced integration. An elastic-plastic isotropic hardening material model was used to represent the Aluminium

7075-T6 bar. The power hardening law:

$$\tilde{\sigma} = H\tilde{\varepsilon}^n \tag{7}$$

was used, where n and H are the strain hardening exponent and the strength coefficient, given in Tab. 1 [12].

3.3 Preliminary FE relaxation analysis

Preliminary FE studies of relaxation were conducted to help estimate the required resolution of the displacement measurement technique. Fig. 3a shows the relaxation displacement along the cutting edge, $x_1 = 0$, for different pin displacement values in the four-point bending test. Based on Fig. 3a, an applied vertical displacement, on the loading rollers of 9 mm was chosen and corresponds to a total applied force of 108 kN.

Relaxation displacements decay exponentially away from the cut, see Fig. 3b. The plots are displacements along x_1 at lines $x_1 = 0$ to $x_1 = c$. The maximum displacement, at the cutting boundary, is around 20 μm. At $x_1 = 0.2c$, the maximum displacement drops to about 12 μm, with most of the data at less than 5 μm. Hence, it is critical to be able to collect the data as close to the cut as possible.

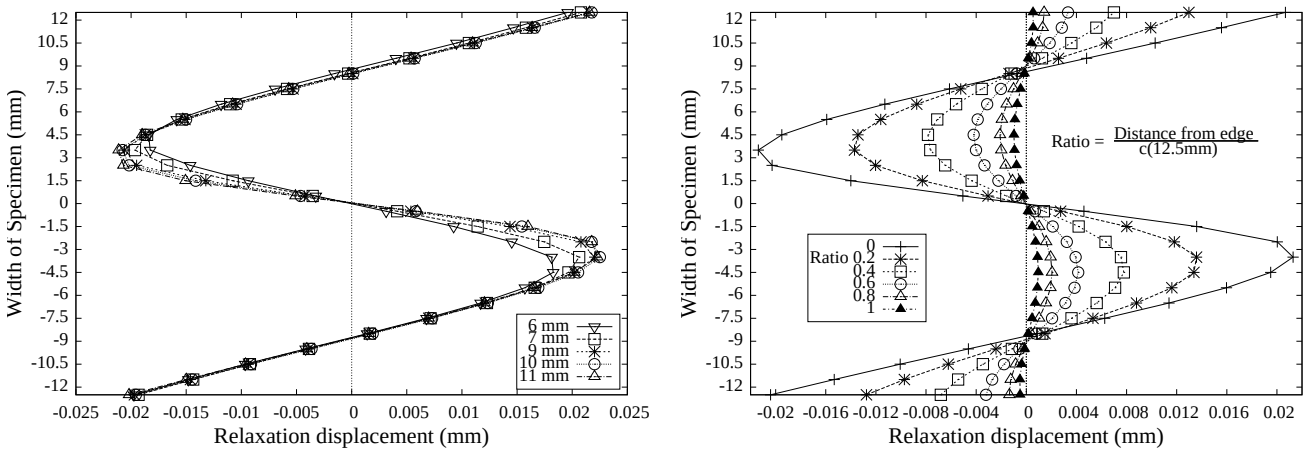

(a) (b)

Figure 3: FE relaxation study for a 25 × 25 mm^2 cross section Al7075-T6 bar under four-point bending, showing: (a) The relaxation displacements at the cutting edge on the side surface for different values of preloading displacement. (b) The relaxation displacements at different distances from the cutting edge for the 9 mm preloading displacement.

3.4 FE analysis of the sensitivity of the method

Prior work [11] makes clear that random experimental errors in the measured displacement can influence the stability of the analytical model. Hence, a good understanding of the stability of the analytical model is required. Fig. 4a shows the FE predicted residual stress field and the stress field reconstructed from the displacements calculated by FE. The peak residual stress to yield ratio is 0.75 in this example. The series expansion was limited to 13 terms. Displacement vectors from all nodes were used, 13,056 points in total. The maximum absolute error is 30.85 MPa. The RMS error is 13.86 MPa and the percentage of RMS error to the peak stress is 3.97%. The agreement between FE predicted and the reconstructed residual stress is good.

Two studies of the sensitivity of the method to the random experimental error were carried out: the effect of random displacement errors on the sensitivity of the reconstructed residual stress, and the relationship between the number and locations of the data points on the accuracy of the reconstructed stresses. Four parameters were investigated: the RMS error, the series limit, the number of data points and the random displacement input error. The percentage of the RMS error to the maximum stress is used as a measure of how well the reconstructed residual stress field fits the FE prediction. The number of data points is linked to the data collection area, see Fig. 4b.

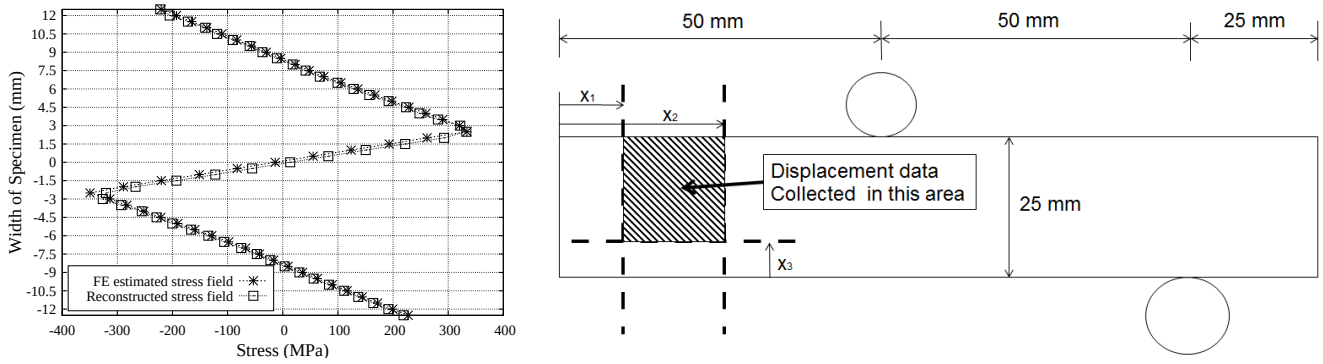

(a) (b)

Figure 4: (a) The 2D FE simulated and the reconstructed residual stress fields for a 25 × 25 mm^2 cross section Al7075-T6 bar under four-point bending. The agreement is excellent. (b) A schematic diagram of the data collection area. x_1, x_2, x_3 are referred to in Fig. 6.

The sensitivity of reconstructed residual stresses to random displacement errors was inves-

tigated. Random errors in displacements in directions 1 and 2 were simulated as

$$u^1_{modified} = (1 + \alpha u_r)\, u^1 \quad , \quad u^2_{modified} = (1 + \alpha u_r)\, u^2 \tag{8}$$

where u_r is a randomly chosen value between -1 and 1, and α is the magnitude of the error. The analysis was carried out with $\alpha = 0.05$, 0.1 and 0.2. Figure 5a shows the result of the sensitivity of the reconstructed residual stress on the error magnitude. Generally, the RMS error increases with the magnitude of the random error. The reconstructed residual stress field is more sensitive to the series limit than to the number of data points, see Fig 5a.

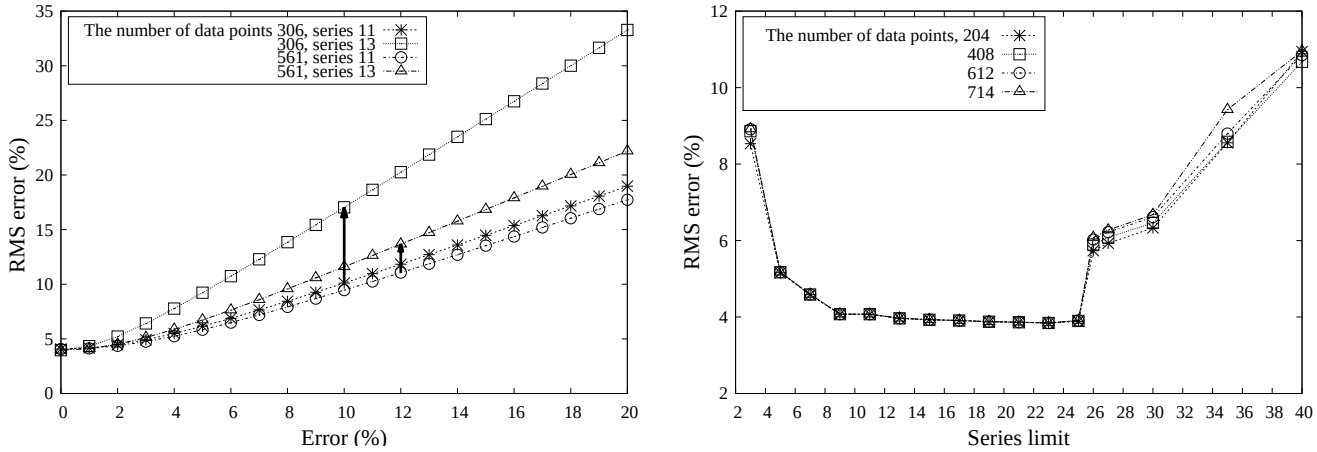

Figure 5: (a) The sensitivity of the reconstructed residual stress to the magnitude of the experimental error. The arrows highlight the change in the RMS error due to the change in the number of terms in the series expansion. The RMS falls with increasing the number of the data points. The number of terms has a greater influence when the number of the data points is smaller. (b) The sensitivity of the RMS to the number of terms in the series expansion for different numbers of the data points. The displacement data is collected from a rectangular region on the side surface. The region extends the full width of the specimen, $x_3 = -12.5$ mm. Along the length of the specimen the region extends from the cut, $x_1 = 0$ mm, to a variable x_2 limit. Refer to Fig. 4b for the description of x_1, x_2 and x_3. Four x_2 values were used: 1.5 mm (204 data points), 3.5 mm (408 data points), 5.5 mm (612 data points) and 6.5 mm (714 data points).

Fig. 5b shows that irrespective of the number of the experimental data points used, the method becomes unstable when the upper limit of the series goes above 25. This investigation

also shows that using just the data from the first 1.5 mm from the cut is enough to reconstruct the residual stresses as long as the upper limit of the Fourier series is between 9 and 25. In all cases the error rapidly increases when the series limit exceeds 25.

It is known that the DIC data from near the edges of the specimen suffers from higher uncertainty [16]. The DIC algorithm can become ill-defined if a fragment of the specimen surface is present in one image, but not in another, which often happens whenever cutting of the specimen is involved. Therefore, it is important to estimate the sensitivity of the method to the emission of a certain region of the surface in the immediate vicinity of the cut, see Fig. 6.

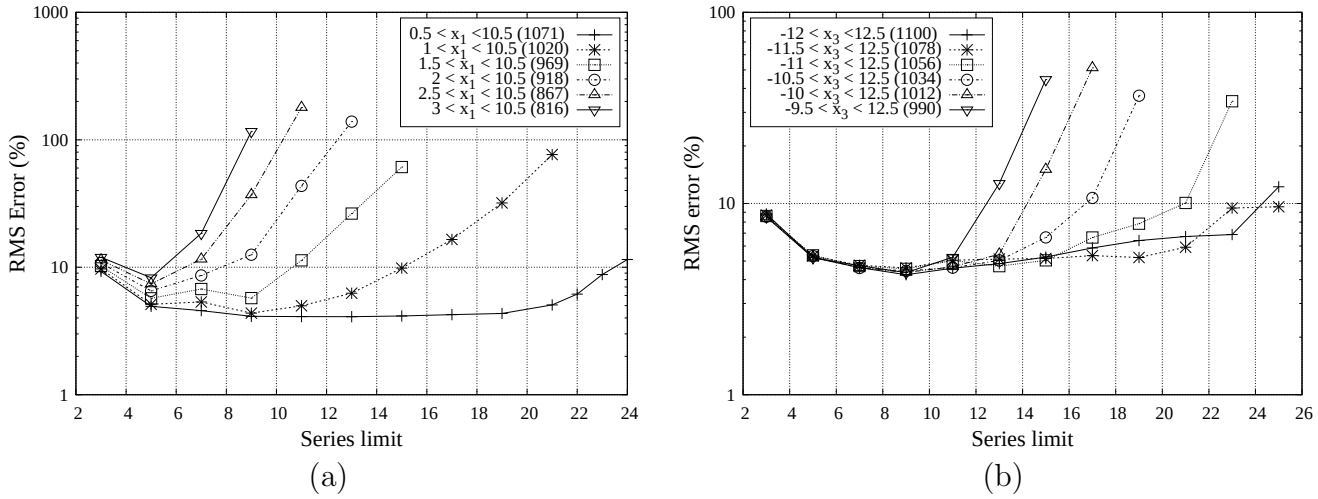

Figure 6: The effect of the Fourier series limit on the RMS for different data collection regions. (a) The region extends the full width of the specimen, but the data points close to the cut are excluded. Refer to Fig. 4b for the description of x_1, x_2 and x_3. (b) The region extends from the cut to 10.5 mm along the axis of the beam. The size of the region in the width direction is given by x_3. The RMS is plotted on the log scale.

The reconstructed residual stress profile is in good agreement with the FE prediction as long as the data closest to the cut is within 1.5 mm. If it is not possible to collect data that close to the cut, the results indicate that the RMS value grows rapidly with the series limit. The reconstructed residual stress field was not significantly influenced by missing displacement data in the region between $x_3 = -12.5$ (the bottom edge) and $x_3 = -9.5$ mm up to the series limit of 11, see Fig. 6b.

4 Experiment

Previous work [11] has indicated that the number of measured displacement points (**M**) is considerably greater than the terms (**N**) in the Mathieu series. As such, **M** / **N** $\gg 10^2$ is required to ensure the stability of the LLS, see Sec. 2. Therefore, in practice, the method requires a full-field measurement technique. In this work DIC is used.

The four-point bending was performed using a 25 × 25 × 250 mm^3 bar machined of Aluminium 7075-T6, see Tab. 1. The bar was plastically bent and unloaded to generate residual stress field between the inner rollers [12]. After unloading, the specimens were cut from both sides successively to a depth of 10 mm on the symmetry plane, $x_1 = 0$ using wire EDM with a diameter of 0.1 mm. The side cut was chosen to minimise plastic deformation, which is discussed in detail in Sec. 6.

To help positioning the specimen after the cut it was not cut completely into two. A small 5 mm ligament was left uncut. The FE analysis of the cut predicted the maximum displacement error to be less than 0.2 μm between the cut to a depth of 10 mm and a complete separation cut. This difference is below the resolution limit of the optical system used, Sec. 4.1, and hence can be neglected.

Material	Yield Stress (MPa)	Modulus of Elasticity (MPa)	UTS (MPa)	Poisson's Ratio	Strength Coefficient (MPa), H	Strain Hardening Exponent, n
Al 7075-T6	503	71700	572	0.33	827	0.113

Table 1: Material properties

4.1 Optical system & Surface preparation

The relaxation displacement expected in this experiment was estimated to be in the order of 10 μm in Sec. 3.3. High displacement resolution requires high magnification, hence very short working distances, in the order of 100-200 mm, were used in this case. Such short working distances make the use of 3D DIC not feasible because of practical limitations of fitting two cameras and a light within a very confined space [17]. Hence 2D DIC is used in this work.

The DIC system consisted of a 10-bit 1392 × 1040 pixel CCD from Dantec dynamics [18]. Fixed focus optics and ring light illumination, both from Navitar [19], were used. The nominal

working distance was 175 mm, giving a 10.6 × 8.0 mm^2 field of view. This optical system gives 7.6 μm/pixel spatial resolution. Istra 4D DIC software was used [18]. Generally, the accuracy of sub-pixel resolution algorithms varies between 0.5 and 0.01 pixel [20]. The corresponding spatial resolution is thus between 0.08 and 4 μm/pixel.

The accuracy of the DIC depends upon suitable surface preparation [21]. Preserving the surface during the EDM cutting is critically important to enable the cross-correlation of the surface images. A random pattern of light scratching applied to Aluminium surface with P180 sand paper has proven to be very effective on Aluminium previously [22]. The same method is used here, see Fig. 7a. Due to the small size of the field of view, four vertical overlapping images were recorded along both sides of the cut in order to capture the whole width of the specimen. The eight images are shown schematically in Fig. 7b. The four vertical adjacent displacement fields of both sides of the cut were processed together as a single dataset.

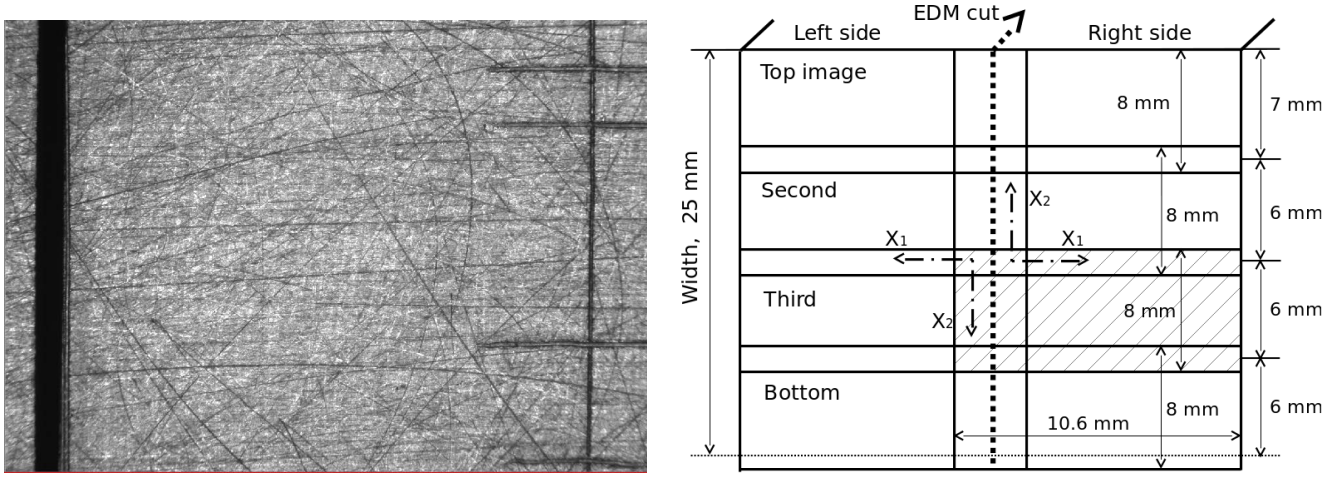

(a) (b)

Figure 7: (a) The surface pattern resulting from light random scratching with P180 sandpaper, illuminated by a ring light source. The image shows a 10.6 × 8.0 mm^2 surface fragment. (b) The layout of 8 overlapping 10.6 × 8.0 mm^2 surface images, with the cut at longitudinal midsection. The hatched area corresponds to the photo on the left.

4.2 Neutron diffraction experiment

The through-depth distribution of residual stress in a nominally identical four-point bend specimen was determined using the SALSA neutron diffractometer at the Institut Laue-Langevin,

France [23]. To achieve this, the inter-planar spacing of the Al {311} lattice plane family was measured in three orthogonal directions (corresponding to the directions of the specimen coordinate axes defined in Fig. 1b) at 11 locations through the depth of the beam at its mid-thickness. An incoming neutron wavelength of 1.644Å was used to give a scattering angle of $2\theta \approx 84.5°$ and hence produce a roughly cuboid scattering volume. The scattering volume itself was defined using collimators to be $2 \times 2 \times 2$ mm^3 in size for all measurements. Lattice parameter measurements from the four-point bend specimen were compared with measurements from an unstressed reference specimen of the same material in order to determine elastic strain. Plane-specific elastic constants (given in [24]) were then used to calculate the residual stresses in the measurement directions at each point via Hooke's law. Statistical uncertainty in the determination of diffraction peak positions was propagated through the calculation of strain and stress using the method described by Wimpory et al. [25, 26]. It should be noted, however, that the resulting uncertainty values do not account for other sources of uncertainty such as errors in specimen alignment and elastic constant determination.

5 Results

The four stitched displacement images, produced in one of the experiments, are shown in Fig. 8a. There are horizontal discontinuous lines due to imperfect stitching and rigid body compensation. Also, note a few white spots at the edges where the DIC correlation failed, probably due to damage to the surface suffered during the EDM cutting. Application of DIC at the image edges is always complicated because some material information is present in one image, but not in the other, e.g. a bit of material surface moves into the field of view after the cut, that was not there before the cut.

The neutron diffraction results and the FE prediction agree well in the mid-thickness, see Fig. 8b. The maximum and the mean absolute error are 80 MPa and 38.15 MPa respectively. Fig. 8b also shows that the FE predicted residual stress on the surface is substantially different from that in the interior.

A single cut can produce four displacement data sets (left and right sides of the cut, and front and rear of the specimen). Fig. 8b shows the reconstructed residual stress field obtained from the measured displacement, see Fig 8a, at the right side of the front surface. A large tail

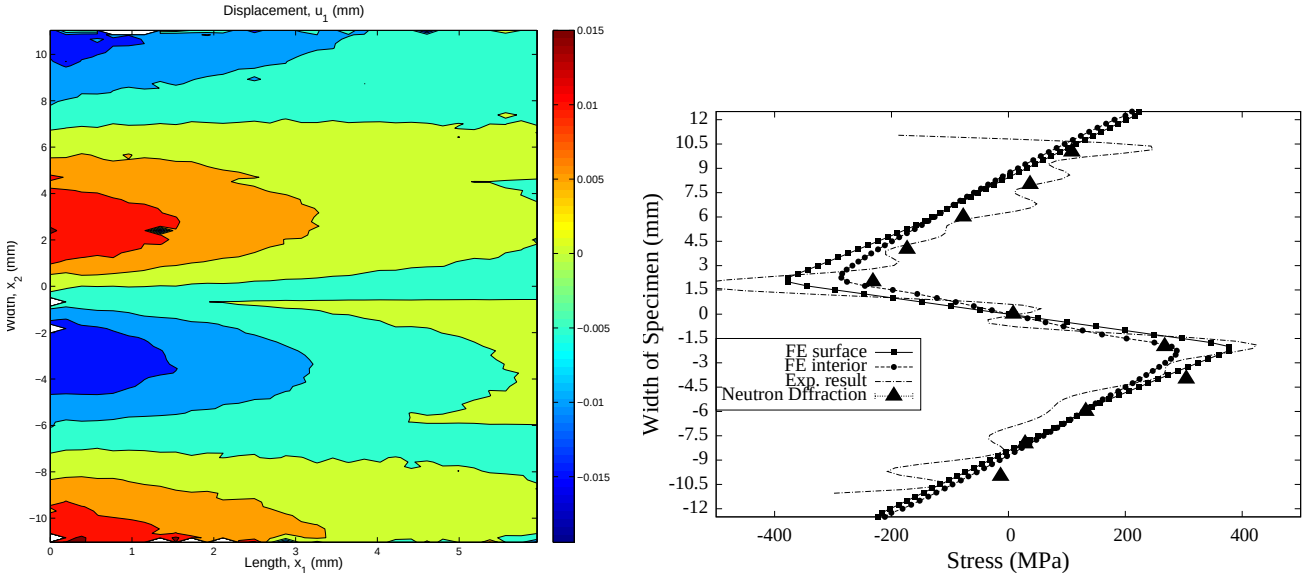

(a) (b)

Figure 8: (a) The measured horizontal displacement field, u_1 (mm). The DIC subset size was 25×25 pixels with no overlap. Horizontal discontinuities are likely due to imperfect stitching. (b) The residual stress profile, reconstructed from the DIC measured displacements, is compared against the FE prediction and the neutron diffraction measurement. The mean statistical uncertainty in the diffraction peak fitting implies a stress uncertainty of approximately 6 MPa.

at the upper edge is likely due to lost displacement data at the very edge (compare with the edge of Fig. 8a. The oscillations are likely caused by the noise in the measured displacement field in Fig. 8a. However, the reconstructed residual stress shows a good overall agreement with that predicted by the FE, see Fig 8b. A similar result was obtained by previously on Aluminium 2024-T4 [27].

6 Study of plastic flow on cutting

During cutting residual stress redistributes in such a way that the force and momentum equilibrium are always satisfied. Although slitting, or EDM cutting, might cause local plastic deformation in the immediate vicinity of the cutting edge, a greater concern is global plastic flow, affecting the redistribution of residual stress, potentially far from the cutting edge. This non-local plastic flow has been observed experimentally and predicted numerically for a variety of MSR techniques, particularly when the residual stress magnitude is close to yield, see e.g. [6–10].

For the slitting method in particular, as the cut propagates into the stressed material, the stresses will increase somewhere else, typically at the cut tip, to preserve the momentum equilibrium [8, 28]. This method is similar to the slitting method in that the cut is progressed normal to the main axis of the specimen. However, in contrast to the slitting method, the cut can be introduced either from the top or from the side surface.

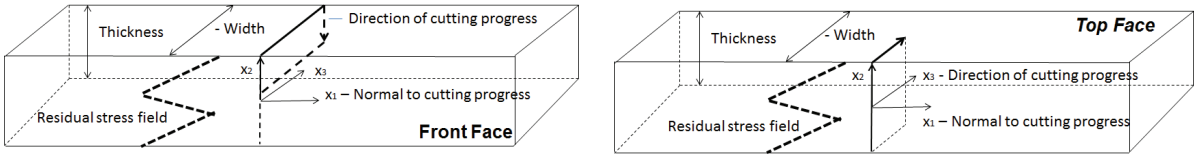

(a) (b)

Figure 9: The two cutting schedules for a prismatic bar analysed in this work. The zigzag dashed line schematically illustrates the residual stress profile produced by four-point bending. (a) The conventional slitting method, e.g. from [8], representing the wire advancing along x_2, from the top face towards the bottom face. The stress along the cutting edge is constant. (b) Slitting along x_3, from the front face to the rear face. The stress along the cutting edge is non-uniform [28].

To measure the four-point bending stress field, the conventional slitting method introduces the slit along x_2, the thickness direction, see Fig. 9a. For such direction of cutting propagation, each slit increment removes a strip of material with a constant stress along the cutting edge, potentially leading to plastic flow if the stresses at that depth are close to yield. In contrast, in this work, the cut is introduced along x_3, the width direction, see Fig. 9b. When the slot is advanced along x_3, it removes a layer of stressed material with non-uniform, self-equilibrated stress profile along the cutting edge. Hence, a zero residual force is removed and potentially, little redistribution of residual stress is caused. The end result is the same in both cases: the specimen is cut on the $x_1 = 0$ symmetry plane. However, the hypothesis is that different amounts of plastic flow are induced depending on the direction of the propagation of the cut [28].

To prove this, a detailed FE study of plastic flow on cutting was carried out. The detailed FE models are presented in Fig. 10. The residual stress field was generated with the peak stress to yield ratio of 0.75, see Fig. 11b.

6.1 Model generation

Both 2D and 3D FE models were generated to investigate the plasticity effect of different cutting directions using the ABAQUS v6.12 FE package. 3D FE models were specifically designed for side cutting simulation. Due to symmetry, only a half of the specimen was modelled in the 2D case and a quarter in the 3D case. In the 2D model, a half of the beam was represented using 4648 eight-node quadratic plane stress elements with reduced integration. The two plastic and elastic cutting processes were simulated with two different cutting methods: (1) incremental cut of 0.25 mm depth from the top to the bottom face by removing the left end of the elements that have x_1 symmetry boundary condition and (2) simultaneous removal of all boundary conditions on $x_1 = 0$. Theoretically, if cutting is simultaneous, no plastic flow is generated, see Fig 11a. The physical cutting is a continuous process, occurring at a certain quite low speed of about 1 mm/min. It has been previously suggested that the cutting increments in FE simulation must be smaller than the local plastic zone size [29]. It has been numerically verified that the increment of the cut of 0.25 mm is smaller than the plastic zone size of 0.5 mm when cutting from the top.

The model had three element sizes, see Fig. 10a. The smallest elements, 0.09×0.25 mm^2, were used to simulate cutting. These elements were progressively removed to simulate the cut. The size is based on the diameter of the EDM wire. The element size in the data collection region was 0.50×0.25 mm^2. Finally, the rest of the model was constructed of 0.65×0.25 mm^2 elements.

For the 3D model, the use of a quarter model was sufficient for the FE simulation due to symmetric conditions. Surface relaxation, due to each increment of the cut decays rapidly with cut depth. In section 4, it is mentioned that the maximum relaxation displacement error between a 10 mm deep cut and a complete separation cut was less than 0.2 μm. This is why cutting simultaneously from both front and rear surfaces, implied by the use of a quarter model, will not have an influence on each other. The relaxation on each surface is solely linked to the cut on that surface.

A structured hexagonal 3D mesh with 238,000 eight-node reduced integration elements was used. The element sizes in the 3D model were identical to the 2D model in plane, with the fixed size of 0.25 mm in the third direction, see Fig. 10b. An extra cutting method, an incremental

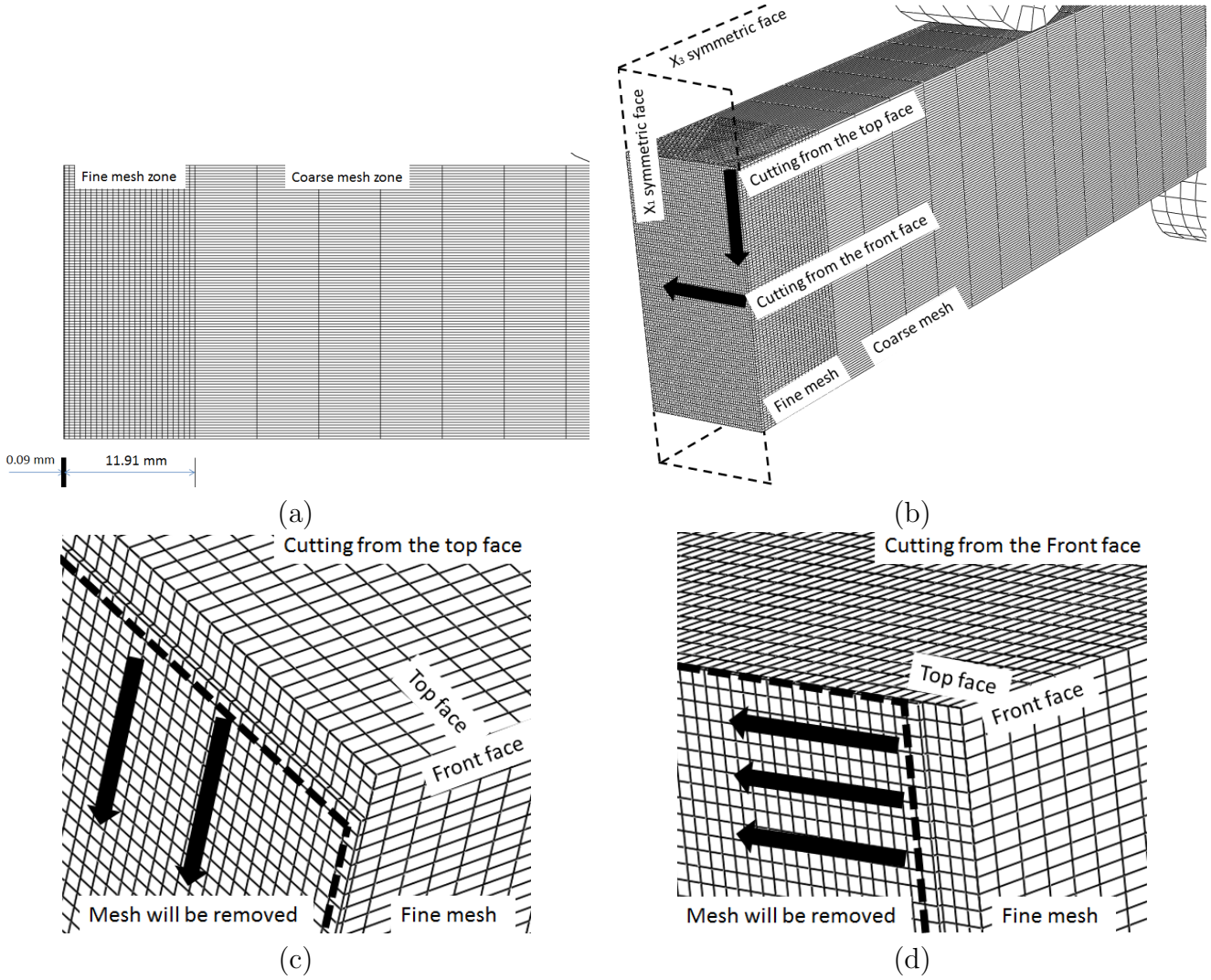

Figure 10: 2D and 3D FE models of four-point bend specimens. (a) 2D half model of the specimen, $x_1 = 0$ is the midsection symmetry plane in the longitudinal direction. The elements on the left model edge are 0.09×0.25 mm^2. These will be removed during the cutting simulation. (b) The 3D quarter model of the specimen, $x_1 = 0$ and $x_3 = 0$ are the symmetry planes. In the cutting process, each layer of the cutting elements was removed either: (c) from the top face toward the bottom face, or (d) from the front face toward the rear face.

cut of 0.25 mm depth from the front face toward the rear face, was performed in the 3D model, see Fig 10d, and compared with the result from cutting from the top face, see Fig 10c.

6.2 Effect of the cutting direction on the plastic flow

Fig. 11 shows the plastic strain caused by stress redistribution from different cutting directions in the 2D and the 3D models. When cutting from the top to the bottom, both the 2D and the

3D models show 0.7% (2D) and 0.8% (3D) equivalent plastic strains at depths between 9 and 13 mm, corresponding to the peak residual stress location. However, when the slit is advanced along the x_3, from the front to the rear face, there is no detectable plastic flow on the front face.

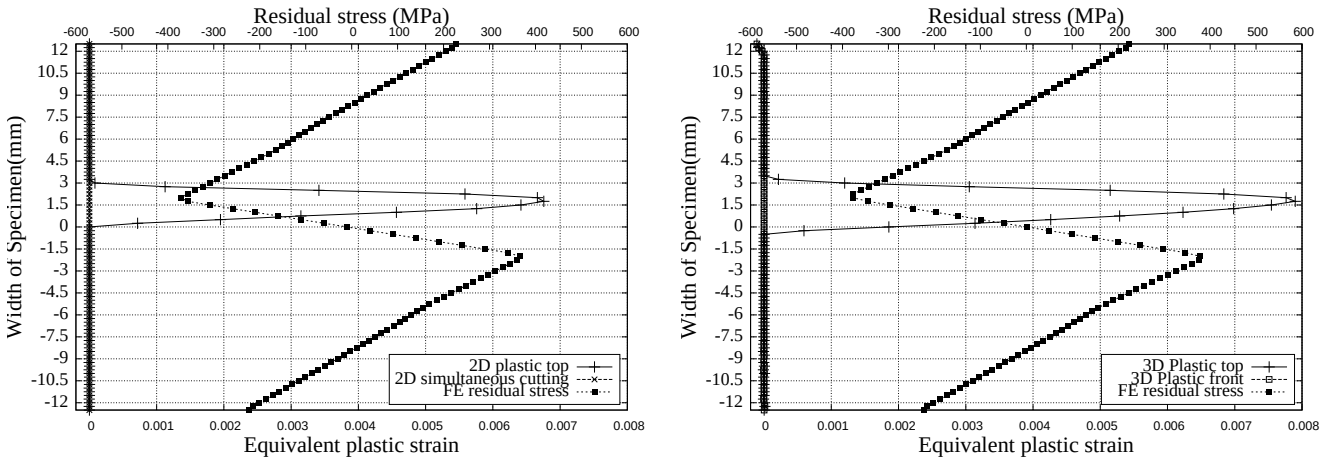

(a) (b)

Figure 11: Plastic flow resulting from different cutting methods. The residual stress field is superimposed for comparison. The equivalent plastic strain profiles through thickness at cutting edge ($x_1 = 0.09$ mm) are shown (a) in the 2D FE model and (b) in the 3D FE model. Only cuts from the top toward the bottom face produce substantial plastic strains in the region of the topmost residual stress peak. The peak residual stress to yield ratio is 0.75.

Fig. 12 shows the 2D surface relaxation displacement field from the two different cutting methods. The distortion at the position of the compressive peak stress is caused by plastic strain, when the cut is advanced from the top, see Fig. 12a.

Using the surface displacement data obtained by the various cutting methods, the residual stress profiles were reconstructed using the analytical method of section 2. The residual stress profiles obtained for an elastic cut from the top face and for an instantaneous elastic-plastic cut match very well with the FE prediction, see fig. 13a. The maximum and mean absolute errors are only around 20 MPa and 6 MPa respectively, which corresponds to a 2% RMS error of the peak stress. However, for the plastic cutting from the top face, there is discrepancy in the region of the residual stress peak where the plastic flow is induced and the maximum and the mean absolute errors are around 124 and 16.6 MPa respectively. The percentage of RMS error to the peak stress is 7.5%, see Fig 13a. The plastic strain occurs at the compressive stress

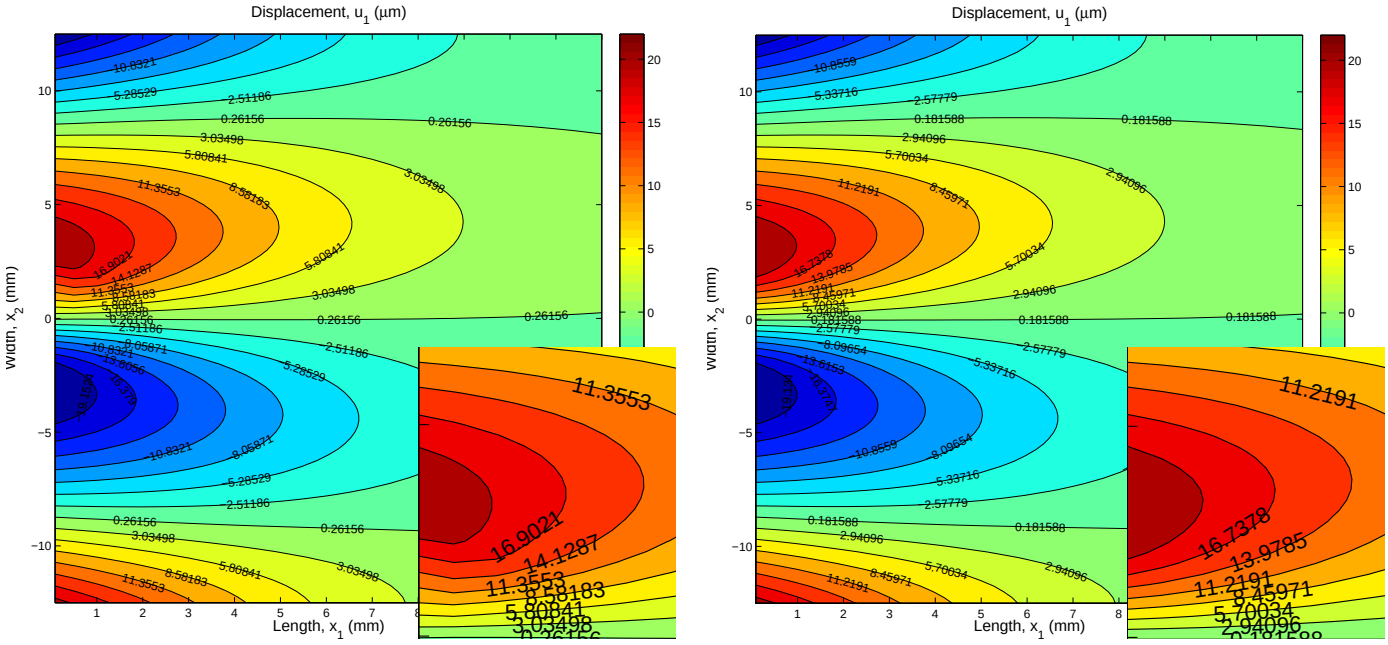

Figure 12: Two surface displacement fields in the region from $x_1 = 0.09$ (cutting edge) to 10 mm obtained from the 2D model. (a) The cut was made progressively from the top face to the bottom face. Induced plastic strain causes distortion of the relaxation displacement field around the top tensile peak. (b) The cut was made via instantaneous removal of all boundary elements. There is no induced plastic strain and hence no distortion of the relaxation displacement field.

peak. Cutting from the bottom causes plastic strain at the tensile stress peak, see Fig 13b.

A 3D model was used to investigate further the directional effect of the cut on the reconstructed residual stress. The side cut displacement data produces the residual stress profile that matches that obtained from the displacement data from the instantaneous removal of the boundary condition, see Fig. 14a. Indeed, this is the expected result since cutting from the side results in no induced plastic strain, see Fig. 13. The percentage of the RMS value to the peak stress is 19%. However, using the relaxation displacement produced in a top cut gives a noticeable discrepancy in the reconstructed residual stress profile, specifically around the first peak, see Fig. 14a, which is caused by the induced plastic strain, see Fig. 11b. The percentage of the RMS error to the peak stress increases to 25%. However, all three 3D reconstructed residual stress profiles disagree with the FE prediction regardless of the cutting method, see Fig. 14a. This can be traced back to different surface displacements in the 2D and the 3D models. Compare Figs. 12 and 14b.

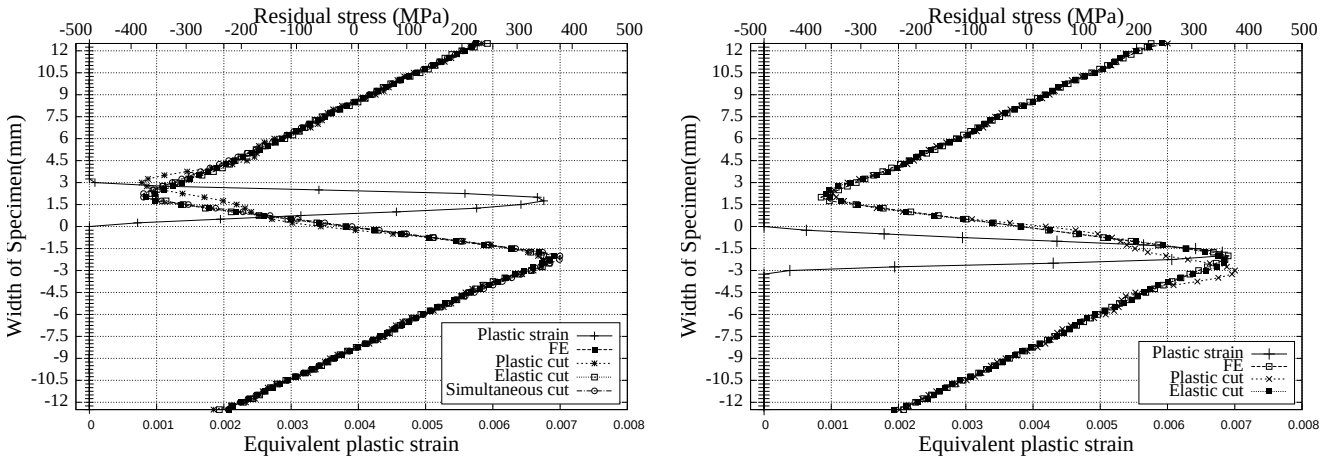

Figure 13: 2D reconstructed residual stress fields obtained via different cutting methods. The equivalent plastic strain, induced along $x_1 = 0.09$ (the cutting edge), is superimposed for comparison. (a) The cut was advanced from the top face. The reconstructed residual stress obtained from incremental elastic cutting and via instantaneous cutting from the top face agree very well with the FE prediction. However, incremental plastic cutting does not agree with the FE prediction, due to induced plastic strain in the region of the compressive residual stress peak. (b) The cut was advanced from the bottom face. Note that the plastic strain is now induced in the region of the tensile residual stress peak.

7 Concluding remarks

The analytical series solution for a semi-infinite 2D strip with self-equilibrated loading at the end was applied in this work to the experimental measurement of four-point bend residual stress field. The specimens were cut from both sides successively to a depth of 10 mm with a wire EDM and the relaxation was measured with DIC. High magnification 2D DIC proved successfully robust and sensitive in capturing the relaxation displacements with sub-pixel resolution algorithms.

The analysis of the plastic flow on relaxation shows that different cutting schedules, which produce the same cut orientation and geometry, cause a different amount of plastic flow. In this work, in the specific case of a four-point bend residual stress field, when the cut is advancing from the top face, each cut removes the layer of material with uniform stress. This leads to stress redistribution across the whole remaining ligament ahead of the cutting edge. Thus, non-negligible plastic strains were caused in the regions with high initial residual stress

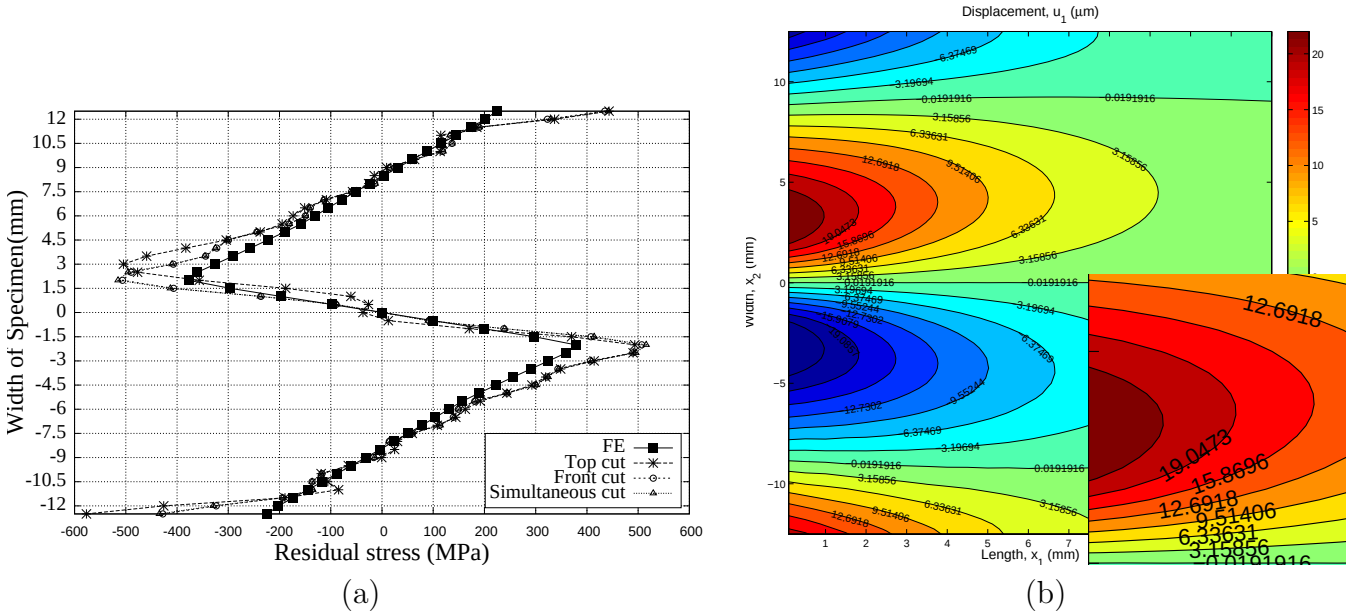

(a) (b)

Figure 14: (a) The reconstructed residual stress fields obtained from the surface displacement data from the 3D model. A disagreement between the top cut and the other cuts is still present, but the magnitude of the peak residual stress is greater than the FE estimate regardless of the cutting method. (b) The surface displacement data from the 3D front cut. No distortions are detectable but the magnitude of peak displacement value differs by about 10% compared with the 2D prediction, see Fig. 12.

magnitude. In contrast, when the cut is advanced from the front face, each increment removes *self-equilibrated* stress, and thus a zero total increment of force. This leads to no stress redistribution, and hence to no plastic flow. This result means that the cut must match not only the chosen analytical model, but also, in some way, to the expected residual stress field. In other words, if there is some prior knowledge of the expected residual stress, then methods based on different cutting schedules will have different success.

In this work, the specimen was not clamped while being cut. However, it is suggested in the literature [9, 10, 30] that different clamping regimes could lead to different plastic deformations and that very rigid clamping as close as possible to the cut could reduce errors in the reconstructed residual stress field. Clamping will be investigated in future work.

The use of a 2D DIC system required to achieve high spatial resolution for this experiment, see Sec. 4.1, led to two practical imaging problems: an inability to distinguish out-of-plane from in-plane motion and a need for correct matching of images of adjacent fragments of the specimen surface. Both of these problems were resolved to some degree via the use of mechan-

ical compensation and post-processing. However, it could be possible that the uncertainty in displacement caused by these two technical issues can be reduced further with the use of a high resolution rigid positioner. Also, it might be beneficial to perform a rigid body correction on all images together [17, 27].

Assuming that the sub-pixel resolution limit is 0.5 pixel, as mentioned in Sec. 4.1, our optical system can resolve displacements of 4μm/pixel. Such resolution is quite low for relaxation measurements on Aluminium. Indeed the extra displacements caused by plastic deformation are on the limit of the resolution of this system. Although the 0.5 pixel limit is the lower bound, and the resolution could be as high as 0.01 pixel, or 0.08μm/pixel for our system, we do not think it is justified to make a stronger quantitative case on the residual stress error due to plastic flow. A higher resolution optical system is recommended for future work.

The accuracy and resolution of the DIC method also critically depend on a multitude of factors, such as specimen surface preparation, illumination, DIC subset size and overlap, etc. However, there is very little definitive advice published in open literature. Often nothing can be recommended apart from some preliminary experimentation to determine the optimum values of these parameters. This is particularly true for the combination of surface finish, illumination and image resolution. Once an image is obtained, it is possible to subject it to quantitative analysis and determine its suitability for DIC experiments [31]. However, very little can be said for sure prior to that.

Although a scratch pattern was found to be very effective in this work, the use of high quality air brush should be explored as an alternative. The airbrush can produce uniform random speckle pattern relative to the pixel size in the image with uniform light intensity [21].

A balance between the accuracy and the spatial resolution is achieved via finding the optimal subset size and step size. Again, these parameters require a trial and error approach. Larger subset sizes lead to more accurate results on average at the expense of not resolving sharp gradients, while smaller subset sizes allow to resolve higher gradients while lowering the accuracy and increasing the noise.

Neutron diffraction was used to validate the FE prediction of residual stress at mid-thickness. The agreement was very good. This provided additional confidence that the FE predictions of surface residual stress is also correct.

The analytical model is 2D, i.e the stress field is assumed constant through the thickness. However, the FE modelling shows that the residual stress at the surface differs from that at mid-thickness. As such, the use of surface displacements in a 2D model leads to errors in the reconstructed stress. This problem was particularly prominent in this work because the thickness was equal to height (square cross section of the bar). Therefore, the method should work better on relatively thinner components.

Finally, prior research suggests that raw displacement data filtering is essential for the use of the inverse method [32]. This will be investigated and might reduce error in reconstructed residual stress.

8 Acknowledgments

The contribution of Dr Thilo Pirling to the diffraction measurements is gratefully acknowledged. Neutron instrument time was provided by the Institut Laue-Langevin under proposal no. 1-02-148.

References

[1] Schajer, G.S., Steinzig, M.: Full-field calculation of hole drilling residual stresses from electronic speckle pattern interferometry data. Experimental Mechanics **45** (2005) 526–532

[2] Ribeiro, J., Monteiro, J., Lopes, H., Vaz, M.: Moire Interferometry Assessement of Residual Stress Variation in Depth on a Shot Peened Surface. Strain **47** (2011) E542–E550

[3] Whitehead, P., Lord, J., Penn, D.: The application of digital image correlation for measuring residual stress by incremental hole drilling. Applied Mechanics and Materials **13-14** (2008) 65–73

[4] Schajer, G., Prime, M.: Use of inverse solutions for residual stress measurements. Journal of Engineering Materials and Technology-Transactions of the ASME **128** (2006) 375–382

[5] Beghini, M., Bertini, L., Raffaelli, P.: Numerical-analysis of plasticity effects in the hole-drilling residual-stress measurement. Journal of Testing and Evaluation **22** (1994) 522–529

[6] Lin, Y.C., Chou, C.P.: Error induced by local yielding around hole in hole drilling methond for measuring residual stress of materials. Materials Science and Technology **11** (1995) 600–604

[7] Mahmoudi, A.H., Truman, C.E., Smith, D.J., Pavier, M.J.: The effect of plasticity on the ability of the deep hole drilling technique to measure axisymmetric redidual stress. International Journal of Mechanical Sciences **53** (2011) 978–988

[8] Prime, M.B.: Plasticity effects in incremental slitting measurement of residual stresses. Engineering Fracture Mechanics **77** (2010) 1552–1566

[9] Shin, S.H.: FEM analysis of plasticity-induced error in measurement of welding residual stress by the contour method. Journal of Materials Science and Technology **19** (2005) 1885–1890

[10] Prime, M.B.: Cross-sectional mapping of residual stresses by measuring the surface contour after a cut. Journal of Engineering Materials and Technology **123** (2001) 162–168

[11] Razumovskii, I.A., Shterenlikht, A.L.: Determining the locally-nonuniform residual-stress fields in plane parts by the sectioning method. Journal of Machinery Manufacture and Reliability *C/C of* Problemy Mashinostroeniia i Nadezhnosti Mashin **4** (2000) 40–45

[12] Dowling, N.E.: Mechanical Behavior of Materials: Engineering Methods for Deformation, Fracture, and Fatigue. 4th edn edn. McGraw-Hill series in materials science and engineering. Prentice Hall (1999)

[13] Timoshenko, S., Goodier, J.N.: Theory of Elasticity. 3 edn. McGraw-Hill (1970)

[14] Hewitt, E., Hewitt, R.E.: The gibbs - wilbraham phenomenon: an episode in fourier analysis. Archive for history of Exact Sciences **21** (1979) 129–160

[15] Dassault Systèmes: Abaqus FEA (2009) http://www.simulia.com/products/abaqus_fea.html (HTML).

[16] Schreier, H.W.: Systematic errors in digital image correlation caused by intensity interpolation. Optical Engineering **39** (2000) 2915

[17] Sutton, M.A., Yan, J.H., Tiwari, V., Schreier, H.W., Orteu, J.J.: The effect of out-of-plane motion on 2D and 3D digital image correlation measurements. Optics and Lasers in Engineering **46** (2008) 746–757

[18] Dantec Dynamics: ISTRA 4D Software Manual Q-400 system (2012)

[19] Navitar: Precise Eye Performance Specifications (2013) http://www.navitar.com/pdf/pe_performance_specs.pdf (HTML).

[20] Pan, B., Xie, H.m., Xu, B.q., Dai, F.l.: Performance of sub-pixel registration algorithms in digital image correlation. Measurement Science and Technology **17** (2006) 1615–1621

[21] Berfield, T., Patel, J., Shimmin, R., Braun, P., Lambros, J., Sottos, N.: Micro-and nanoscale deformation measurement of surface and internal planes via digital image correlation. Experimental Mechanics **47** (2007) 51–62

[22] Lopez-Crespo, P., Shterenlikht, A., Yates, J.R., Patterson, E.A., Withers, P.J.: Some experimental observations on crack closure and crack-tip plasticity. Fatigue & Fracture of Engineering Materials & Structures **32** (2009) 418–429

[23] Pirling, T., Bruno, G., Withers, P.J.: SALSA - A new instrument for strain imaging in engineering materials and components. Materials Science and Engineering: A **437** (2006) 139–144

[24] Hutchings, M.T., Withers, P.J., Holden, T.M., Lorentzen, T.: Introduction to the characterization of residual stress by neutron diffraction. CRC press (2005)

[25] Wimpory, R.C., Ohms, C., Hofmann, M., Schneider, R., Youtsos, A.G.: Statistical analysis of residual stress determinations using neutron diffraction. International Journal of Pressure Vessels and Piping **86** (2009) 48–62

[26] Wimpory, R.C., Ohms, C., Hofmann, M., Schneider, R., Youtsos, A.G.: Corrigendum to "Statistical analysis of residual stress determinations using neutron diffraction". International Journal of Pressure Vessels and Piping **86** (2009) 721

[27] Kim, H.K., Pavier, M.J., Shterenlikht, A.: Measuring locally non-uniform in-plane residual stress with straight cuts and DIC. (In: Proceedings of 9th International Conference on Advances in Experimental Mechanics, 3-5 September 2013, Cardiff, Wales, UK)

[28] Kim, H.K., Pavier, M.J., Shterenlikht, A.: Plasticity and stress heterogeneity influence on mechanical stress relaxation residual stress measurements. (In: Proceedings of 9th European Conference on Residual Stresses, 7-10 July 2014, Troyes, France)

[29] Simandjuntak, S., Alizadeh, H., Smith, D.J., Pavier, M.J.: Three dimensional finite element prediction of crack closure and fatigue crack growth rate for a corner crack. International Journal of Fatigue **28** (2006) 335–345

[30] Traore, Y., Bouchard, P.J., Francis, J., Hosseinzadeh, F.: A novel cutting strategy for reducing plasticity induced errors in residual stress measurements made with the contour method. (In: Proceedings of the ASME Pressure Vessels and Piping Conference, PVP2011, Vol 6, A and B, New Your, USA)

[31] Lane, C., Burguete, R.L., Shterenlikht, A.: An objective criterion for the selection of an optimum DIC pattern and subset size. (In: Proceedings of the 2008 SEM Annual Conference, Orlando, Florida, USA, Paper 297)

[32] Kartal, M.E.: Analytical solutions for determining residual stresses in two-dimensional domains using the contour method. Proceedings of the Royal Society A-Mathematical Physical and Engineering Sciences **469** (2013)